Fabrication of a two-step thermoresponsive ultrafiltration membrane via polymerization of a lyotropic liquid crystal

Younes Saadat [1], Kyungtae Kim [2], Reza Foudazi [1*]

[1] *School of Chemical, Biological and Materials Engineering, The University of Oklahoma, Norman, OK 73019, USA*

[2] *Materials Physics and Applications Division, Center for Integrated Nanotechnologies, Los Alamos National Laboratory, Los Alamos, NM 87545, USA*

ABSTRACT

In this work, we present the fabrication of a two-step thermoresponsive ultrafiltration (UF) membrane through polymerization of a lyotropic liquid crystal (LLC). A mixture of commercially available Pluronic F127 block copolymer, water (containing ammonium persulfate as the initiator), and polymerizable oil (n-butyl acrylate/ethylene glycol dimethacrylate) is used to create an LLC with lamellar structure, as characterized by cross-polarized light microscopy and atomic force microscopy. Differential scanning calorimetry is employed to evaluate the thermoresponsive behavior of the polymerized LLC (polyLLC). Two-step thermoresponsiveness (~35 °C and ~50 °C) of the polyLLC is observed due to the lower critical solution temperature (LCST) of F127 and melting of the crystalline structure of the polyethylene oxide (PEO) chains of the F127 surfactant. In the next step, the obtained mesophase is cast on a nonwoven polyester support sheet followed by thermal polymerization. The hydration capacity, water flux, water flux recovery after fouling, and molecular weight cut-off (MWCO) of the obtained membrane are evaluated at different temperatures to examine its thermoresponsiveness. The experimental results reveal that the UF membrane has a reversible thermoresponsive behavior at the LCST and PEO melting of polyLLC. Additionally, cleaning efficiency of the fouled membrane can be enhanced by using its thermoresponsive behavior, resulting in an extended lifetime of the product. Furthermore, the MWCO of the membrane can be altered with temperature due to the pore size change with temperature stimulus.

Keywords: *Thermoresponsive membranes, Lyotropic liquid crystals, Mesophases, Thermal polymerization, Self-assembly*

[*] Corresponding author. Email: rfoudazi@ou.edu.

1. INTRODUCTION

Demand for clean water is continuously increasing with the growth of human population. Membrane technology is the most efficient and versatile approach to purify different water resources (e.g., brackish water, seawater, and wastewater) for fulfilling this demand [1]. Microfiltration, ultrafiltration (UF), nanofiltration (NF), and reverse osmosis are the main steps to purify water from different contaminants [2]. UF membranes have a key role in this process as they are used for the removal of suspended particles, viruses, bacteria, etc. [3]. In addition to water filtration, UF membranes are vastly used in protein purification, pharmaceutical industries, and food processing [4,5]. However, there is a need for improving the membranes selectivity and permeability simultaneously. For instance, the feed of UF membranes usually contains solutes/particles with different sizes. Therefore, the separation of different components with one UF membrane will be limited. Having a UF membrane with a tunable pore size will address this challenge to a large extent [6]. Moreover, another crucial issue that must be tackled is the fouling of UF membranes, which can decrease the membrane efficiency over time [7,8].

Stimuli-responsive membranes can address the aforementioned challenges and improve the performance of UF membranes [8]. The surface properties and pore structure of these membranes can be altered via an external stimulus, such as temperature [9], pH [10], light [11], electrolyte[12], and magnetic field [13]. This behavior not only results in a tunable pore size and thus dynamic selectivity, but also improves the cleaning efficiency of the membrane after contamination with foulants [14].

Thermoresponsive membranes are of interest because not only implementation of thermal response has less complications in the synthesis, but also temperature changes has usually negligible effect on the chemistry of the feed stream [8]. Additionally, there are a variety of thermoresponsive polymers that can be used for the fabrication of membranes [15]. Non-solvent induced phase separation (NIPS) has been the main technique to produce thermoresponsive membranes. For example, Yu et al. used poly(N-isopropylacrylamide) (PNIPAM)-grafted polyvinylidenefluoride (PVDF) copolymers and reported a dynamic permeability and selectivity of the membrane in response to the temperature changes [16]. By using NIPS process, Chen et al. fabricated membranes of PNIPAM microgels/PVDF blend, which show a similar dynamic behavior with temperature change [17]. Recently, Choi and coworkers used a mixture of polyethersulfone (PES) and in-lab synthesized poly(2-dimethylaminoethyl methacrylate)-block-poly(N-isopropylacrylamide) to form two-step thermoresponsive membranes capable of separating different proteins with temperature [14]. However, the NIPS method used for preparation of these membranes is environmentally questionable as large quantities of organic solvent, as high as 70% (in volume) is required [18]. Additionally, incorporation of in-lab synthesized thermoresponsive polymers in the final membrane makes the final product expensive and impractical for scaleup [14].

Polymerization of lyotropic liquid crystals (LLCs) is an alternative approach to produce nanoporous membranes without using huge volumes of organic solvents [1,19–21]. In this technique, self-assembly of a surfactant in water/oil mixture results in mesomorphic phases

(mesophases) having high extension in one or two dimensions with length scales on the order of 2–50 nm [22]. A nonporous structure of the desired final product can be achieved via polymerization of aqueous phase, oil phase, or the surfactant of LLCs [23]. There are some reports in the literature, in which surfactant or oil phase of LLCs is polymerized to fabricate porous membranes (mainly UF and NF) [3,19,24–26]. Polymerization of aqueous phase of LLCs is also used to produce thermoresponsive hydrogels [27,28]. However, there is no report in the literature on LLC templating process for fabrication of thermoresponsive membranes.

In this work, we present the first successful approach to create two-step thermoresponsive UF membranes from the polymerization of LLCs directed by commercially available F127 block copolymer surfactant, i.e., poly[(ethylene oxide)-block-(propylene oxide)-block-(ethylene oxide)] or PEO-PPO-PEO. F127 is commonly used in drug delivery systems thanks to its thermoresponsive behavior [29]. In combination with water and other components (e.g., acids), this commercially available copolymer, which possess FDA approval [30], can form gels having LCST at about 25-37 °C [31]. Moreover, Holmqvist et al. showed that a mixture of F127, water, and *p*-xylene can create different LLC structures (e.g., lamellar and hexagonal) [32]. Furthermore, Qavi et al. have recently shown the possibility of fabricating UF membranes though the polymerization of LLCs created by Pluronic copolymers. Their work has proved that the chains of Pluronic copolymer remain in the structure of the obtained polyLLC [3]. Inspired by the aforementioned studies, we prepared a polyLLC with lamellar structure from F127 for producing UF membranes with thermoresponsive behavior. The obtained polyLLC exhibited thermoresponsiveness at ~35 and ~50 °C thanks to the lower critical solution temperature (LCST) of F127 and melting of the crystalline structure of poly(ethylene oxide), PEO, chains of the surfactant, respectively. The membrane obtained from the polyLLC showed dynamic permeability in response to the temperature with an excellent reversibility. Furthermore, taking the advantage of this thermal response, it was possible to increase the cleaning efficiency of the fouled membrane. The most important strengths of this work are the use of commercially available raw materials and employing a straightforward processing technique to create two-step thermoresponsive UF membranes.

2. EXPERIMENTAL

2.1. Materials

Pluronic F127 copolymer, PEO_{106}–PPO_{70}–PEO_{106}, with M_w of ~12,500 g/mol was kindly provided by BASF. *n*-Butyl acrylate (*n*BA), ethylene glycol dimethacrylate (EGDMA), ammonium persulfate (APS), and azobisisobutyronitrile (AIBN) were purchased from Sigma-Aldrich and used as received. Deionized (DI) water with a conductivity of 0.055 μs/cm (obtained from EMD Millipore Direct-Q3) was used in all experiments. Bovine serum albumin (BSA) was purchased from Sigma-Aldrich and used as a membrane foulant. For molecular weight cut-off (MWCO) measurements, we used PEO with different molecular weights (100, 200, 300, 400, 600 and 900 kDa) from Sigma-Aldrich. Nonwoven polyester sheets with 2 μm porosity (CraneMat® CU463) were kindly provided by Neenah Filtration and employed as a support layer for membrane

fabrication. Moreover, a commercially available polyacrylonitrile (PAN) UF membrane with a rejection size of 400 kDa was purchased from Sterlitech Corporation (YMPX3001, Synder Flat Sheet Membrane) and used for comparison in this study.

2.2. Preparation of LLC

To prepare the lamellar mesophase, F127, water (containing APS) and oil (*n*BA and EGDMA) were mixed with weight ratio of F127/water/oil 50/20/30. EGDMA and APS concentration was 20 and 7 wt% with respect to *n*BA content, respectively. Briefly, all the components were mixed in a 50 ml centrifugal tube by hand mixing and centrifugation at 10,000 rpm for 30 min. Until obtaining a transparent gel, the hand mixing and centrifugation were repeated .

2.3. Characterization of LLC and polyLLC

2.3.1. Cross-polarized light microscopy (CPLM)

The birefringence of lamellar LLC structure was examined by a cross-polarized Olympus microscope (model BX60) equipped with a digital camera before and after polymerization. For sample preparation, about 0.2 gr of uncured LLC sample was sandwiched between a glass slide and a glass cover slip. In the case of polyLLC, the test was carried out after curing the LLC at 65℃ for 24 h.

2.3.2. Small angle X-ray scattering (SAXS)

SAXS [33] was used to confirm the structure of the LLC before and after polymerization. Centrifugation was used to load the LLC gel into quartz capillary with a nominal diameter of 1.5 mm (Charles Supper Company, Natick, MA) followed by sealing the capillary with critoseal and epoxy glue. For SAXS analysis of polyLLC sample, the loaded LLC in the capillary tube was cured at 65 °C for 24 h. Two-dimensional (2D) scattering patterns were acquired from a Bruker Nanostar X-ray scattering system equipped with a monochromatic Cu Kα radiation source. Azimuthal integration of the 2D scattering patterns resulted in one dimensional (1D) scattering profiles.

2.3.3. Atomic force microscopy (AFM)

Morphological analysis of polyLLC was performed using AFM. To do so, a piece of polyLLC was placed in liquid nitrogen for 20 min. The frozen sample was broken into small flat pieces for the cross-section observation. AFM studies were carried out on the broken surfaces using the tapping mode of a Bruker Dimension FastScan AFM instrument.

2.3.4. Differential scanning calorimetry (DSC)

DSC was used to study the thermal behavior of pure F127, poly(*n*BA-co-EGDMA), and polyLLC. The poly(*n*BA-co-EGDMA) copolymer was synthesized through the bulk polymerization of the corresponding monomers at 65 °C using AIBN as the initiator and the composition used as the oil phase of LLC. DSC Q2000 (TA Instruments, New Castle, DE) was employed for this study.

Around 30 mg of the desired sample was loaded into a Tzero aluminum pan followed by sealing with a Tzero hermetic lid. The temperature sweep was performed from 0 to 60 °C (and vice versa for F127 and polyLLC) with 1 °C/min ramp. The cycle was repeated twice to erase the thermal history of samples. The results of the second cycle are presented in the paper.

2.4. Preparation of the polyLLC membrane

To polymerize LLC on the support layer (having ~5×5 cm^2 surface area), about 0.8 g of the LLC was sandwiched between pre-cut Mylar films and smooth glass plates, which was subsequently cast under 5 ton pressure for more than 10 min. In the next step, the cast gel on the support was polymerized by heating in the oven at 65 °C for 24 h.

2.5. Characterization of the polyLLC membrane

2.5.1. Hydration capacity

The hydration capacity, which is the maximum water uptake per unit volume (mg/cm^3) of the membrane, was measured according to the available procedure in the literature [9,14]. Briefly, the weight of membrane samples of size 2 cm ×2 cm was determined in dry state as well as in wet state at different temperatures. Then, the dry weight was subtracted from the wet weight, and the obtained number was divided by the volume of the membrane, resulting in the hydration capacity.

2.5.2. Water flux and permeability

We used Sterlitech HP4750 high pressure stirred cell with the effective area of ~ 14.6 cm^2 operating in dead-end filtration mode to measure the membrane flux (reported as $liter/m^2/h$) under stirring at 750 rpm with a magnet stirrer. A nitrogen pressure of 30 psi (~ 2.07×10^5 Pa) was used for the flux measurements. To evaluate the thermoresponsiveness of the membrane, the flux test was carried out at different temperatures from 25 to 60 °C. To do so, the filtration setup containing the membrane was placed in a water bath maintained at the desired temperature with an accuracy of ±0.1 °C. Precise control of the temperature is necessary to have a constant temperature in the membrane level and thus avoid any reduction in the boundary layer due to the heat caused by shear, which can affect membrane performance (e.g., permeability, selectivity, and fouling resistance). The flux at elevated temperatures was measured after ensuring the isothermal condition and having a stable flux. It should be noted that all the measurements were repeated three times. The membrane permeability was calculated based on the obtained experimental results using Darcy's law [3]:

$$\frac{\kappa}{l} = \frac{Q\mu}{A\Delta P} \quad (1)$$

In this equation, Q, μ, A, ΔP, l, and κ are the flow rate, viscosity, membrane area, pressure difference across the membrane, membrane thickness, and Darcy's constant (intrinsic permeability), respectively. The intrinsic permeability was normalized to the membrane thickness to cancel out the effect of thickness variation in our comparisons. It is worth to point out that the following equation [34] was used to calculate the viscosity of water at different temperatures:

$$\mu_w = (1.002\times10^{-3})(10^B) \quad , \quad B = \frac{1.3272(20-T)-0.001053(T-20)^2}{T+105} \tag{2}$$

where μ_w is the kinetic viscosity of water and T is temperature in K.

2.5.3. Evaluation of fouling resistance and cleaning efficiency

The following experimental procedure was followed to determine the fouling resistance of and cleaning efficiency for the membrane:

1) The flux of the membrane was measured by passing DI water through the membrane for 30 min at 25 °C.
2) 1000 ppm aqueous solution of BSA (as the model foulant) was used as the feed stream and the flux was recorded at 25 °C until reaching steady state conditions.
3) The membrane was backwashed with DI water for 30 min at different temperatures: 25, 35, or 50 °C.
4) The fouling-cleaning cycle (i.e., steps 1-3) was repeated three times.

It should be mentioned that the backwashing steps were carried at different temperatures to examine the effect of membrane thermoresponsiveness on the cleaning efficiency.

The reversible (also called cleaning efficiency) and irreversible fouling of the membrane were calculated using the following equations, respectively:

$$Reversible\ fouling\ = \frac{(Flux\ of\ cleaned\ membrane\ -\ Flux\ of\ fouled\ membrane)}{(Initial\ flux\ of\ membrane)}\times100 \tag{3}$$

$$Irreversible\ fouling\ = \frac{(Initial\ flux\ of\ membrane - Flux\ of\ cleaned\ membrane)}{(Initial\ flux\ of\ membrane)}\times100 \tag{4}$$

2.5.4. Molecular weight cut-off measurements

The permeation of 1 mg/mL aqueous solutions of PEO with different molecular weights (100-900 kDa) was studied to determine the MWCO of the membrane. The concentration of PEO in the permeate stream was determined by the total organic carbon analyzer (TOC), Shimadzu (TOC-L series). The PEO rejection was determined by using following equation:

$$r = (1-\frac{C_p}{C_f})\times100 \tag{5}$$

where r, C_p, and C_f are rejection, PEO concentrations in permeate, and PEO concentrations in feed, respectively. MWCO is defined as the molecular weight of the PEO that shows at least 90% rejection [35]. The TOC test was repeated 5 times and the average value is reported in the paper.

To examine the effect of thermoresponsiveness of the polyLLC membrane on the MWCO, the PEO solutions were passed through the membranes at different temperatures and the TOC measurements were performed on the permeates. To cancel out the effect of temperature on the hydrodynamic radius of PEO chains and thus have a precise MWCO results, dynamic light scattering (DLS) measurements on PEO solutions were done at different temperatures. To do so, a Malvern Zetasizer Nano ZS was used with a laser wavelength of 8324 Å and at a scattering angle

of 90°. Solutions of PEO with different molecular weights at a concentration of about 0.1 wt% were used for DLS measurements using the procedure described in the literature [36].

3. RESULTS AND DISCUSSIONS

3.1. Characterization of LLC and polyLLC

As the first step, we needed to characterize the Pluronic/water/oil mixture to confirm the LLC and polyLLC structures created by F127. Structural analysis of the obtained LLC before and after polymerization via CPLM is shown in Fig. 1a, b. The oily-streak texture reveals that the mesophase has the lamellar structure [37]. The absence of extinction (a dark image) in the CPLM photograph of polyLLC indicates that the structure remains birefringent, meaning that we have structure after polymerization. Then we characterized LLC and polyLLC with SAXS. According to the SAXS results (see Fig. 1c), Bragg peaks with ratios of 1:2 is observed for LLC before reaction while only one peak is seen for polyLLC. Additionally, d-spacing of the structure ($d = \frac{2\pi}{q*}$) increases from 11.6 to 20.18 nm after polymerization. The CPLM and SAXS observations reveal that even though we have a nanostructure with bigger domain sizes after polymerization, the parent lamellar structure has partially been retained. To further evaluate the polyLLC structure, AFM studies were carried out. The acquired results are shown in Fig. 1d, e, f. As can be seen in the AFM images, the dried polyLLC sample has a structure in the form of arranged stacks which confirms the presence of lamellar structure. However, the image analysis shows that we have a distribution of layers thicknesses with an average thickness of about 30 nm and standard deviation of 5.9 nm. Such variation in thickness of the layers confirms our observation in SAXS analysis (i.e., partially retaining the parent LLC structure).

After making sure that the polyLLC has the desired nanostructure, we evaluated its thermoresponsiveness via DSC. We not only analyzed polyLLC, but also tested poly(*n*BA-co-EGDMA) and pure F127 to distinguish which component is responsible for probable thermal transitions in the temperature range of 25 to 60 °C. The obtained results are presented in Fig. 2. As can be seen, there is not any thermal transition for poly(*n*BA-co-EGDMA) in this temperature range. However, F127 shows an endothermic peak at around 50-58 °C in the heating cycle, attributed to the melting of PEO crystalline regions. In addition, an exothermic peak is observed starting from 48 °C and ending at about 43 °C in the cooling cycle of F127. This peak can be attributed to the crystallization of PEO chains. In the case of as-synthesized polyLLC (i.e., containing water), two endothermic peaks are observed in the heating cycle. The first peak at about 26-33 °C can be attributed to the LCST of F127, which is consistent with the reported LCST range of F127/water mixtures in the literature [31]. The second peak, observed at about 50 °C, belongs to the melting of PEO crystalline regions in accordance with the DSC of pristine F127. Having an exothermic peak in the cooling cycle also proves the presence of crystallinity in the obtained polyLLC, which can be melted down at 50 °C. The two thermal transitions provide the possibility to induce two-step thermo-responsiveness in the membrane.

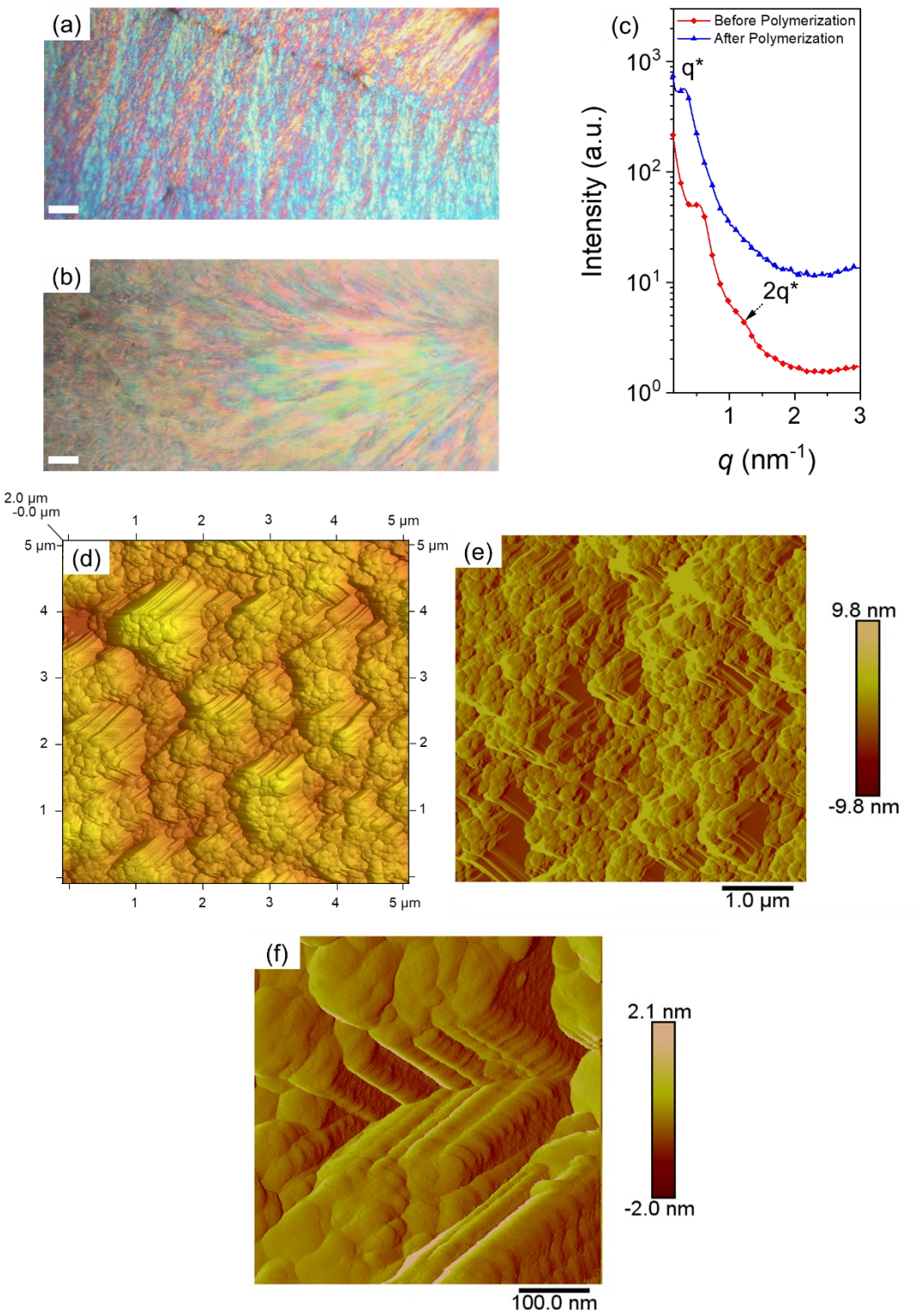

Fig. 1. CPLM images of LLCs with lamellar structure: (a) before and (b) after thermal polymerization (scale bar: 50µm). (c) 1D SAXS data for LLCs before and after reaction (the plots are vertically shifted for clarity). (d and e) AFM micrograph of the cross section of dried polyLLC in a 5 $\mu m \times 5 \mu m$ area; higher magnification is shown in (f).

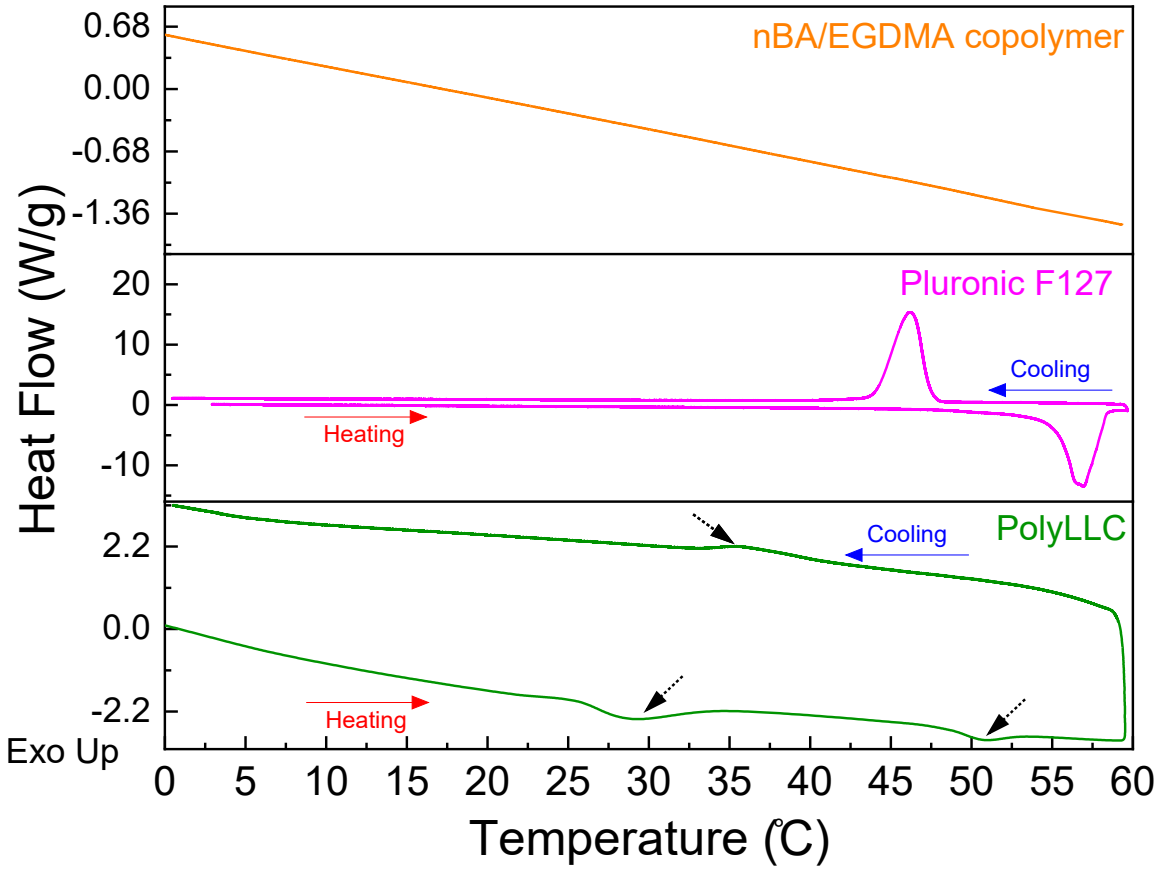

Fig. 2. DSC measurement results for poly(*n*BA-co-EGDMA), F127, and polyLLC.

3.2. Characterization of membranes

As stated in the experimental section, a commercially available non-thermoresponsive PAN membrane was used to compare the results with the polyLLC membrane. The selected PAN membrane had a MWCO of 400 kDa, which is equal to the pore size of about 40 nm based on equation (6) [38].

$$a_{Stokes} = 10.44 \times 10^{-3} M_w^{\ 0.587} \quad (6)$$

Where a_{Stokes} and M_w are Stokes radius in nm and MWCO, respectively. The results of membranes performance evaluation will be discussed in the following sections.

3.2.1. Hydration capacity

Measuring the hydration capacity of a membrane at different temperatures is performed to confirm the thermoresponsiveness [14]. The membrane is called thermoresponsive if its hydration capacity changes by temperature. We measured the hydration capacity for PAN and polyLLC membranes at 25, 35, and 50 °C as shown in Fig. 3. These temperatures were chosen based on the DSC results. While the hydration capacity remains constant for PAN membrane, it has an increasing trend for polyLLC sample. This means that the porosity of polyLLC membrane increases with an increase in temperature. This behavior happens in two steps, which is consistent with the thermal transitions

observed in DSC analysis. It is worth noting that higher hydration capacity of PAN membrane compared to the polyLLC specie can be due to its higher porosity.

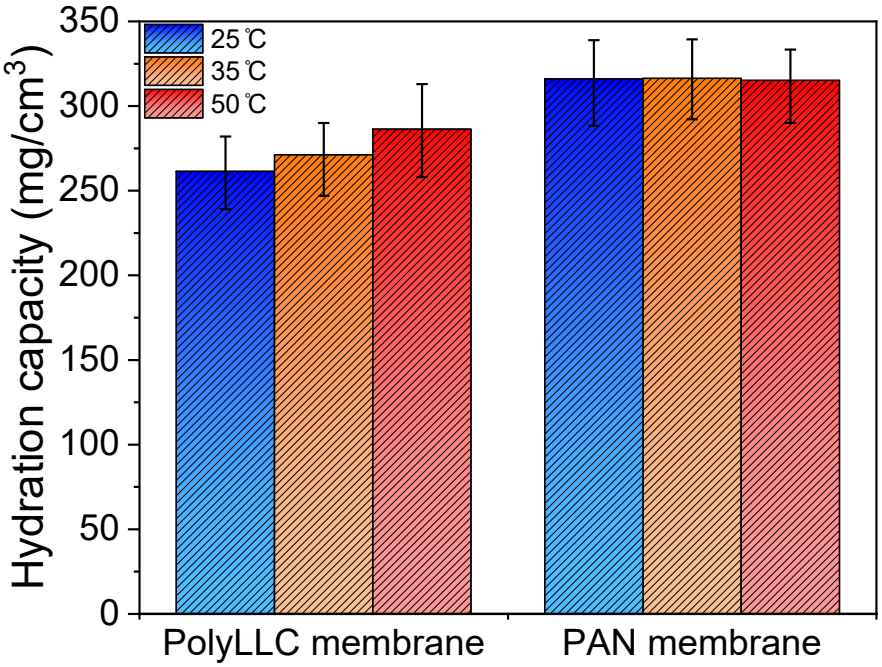

Fig. 3. Changes in hydration capacity for PAN and polyLLC membranes based on the temperature variation.

3.2.2. Water flux and permeability

The water flux changes for PAN and polyLLC membranes versus temperature are shown in Fig. 4a. Both of the membranes show an increasing trend in flux, but polyLLC one shows two steps of increase at 35 and 50 °C. To cancel out the effect of water viscosity decrease with temperature on the results, we also plotted permeability, κ/l, versus temperature (see Fig. 4b). As can be clearly seen, the permeability of PAN membrane is almost constant at different temperatures, meaning that the reason of ascending water flux trend for PAN was the decrease in the water viscosity. However, the polyLLC membrane still maintains the two-step increase in the permeability. These transitions are in well agreement with the results of DSC analysis as well as the hydration capacity measurements. One important observation which must be considered here is that the second transition has more effect on the permeability (~ 14% increase) compared to the first transition (~8.5% increase). Therefore, the pore size increase is higher when the polyLLC loses its crystallinity rather than when the LCST transition of F127 takes place. In the following sections, we will elaborate the mechanism of two-step thermoresponsive behavior, where we will suggest that the crystallinity of the PEO blocks and rearrangement of F127 chains are its root causes. This conclusion can be further confirmed via MWCO measurements.

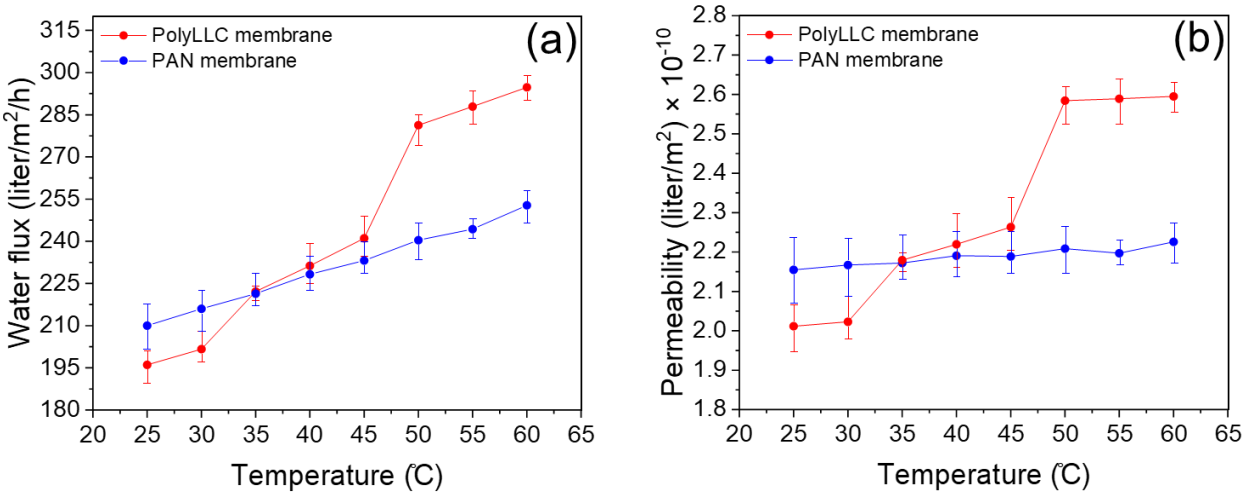

Fig. 4. Changes in (a) water flux and (b) permeability for PAN and polyLLC membranes based on the temperature variation.

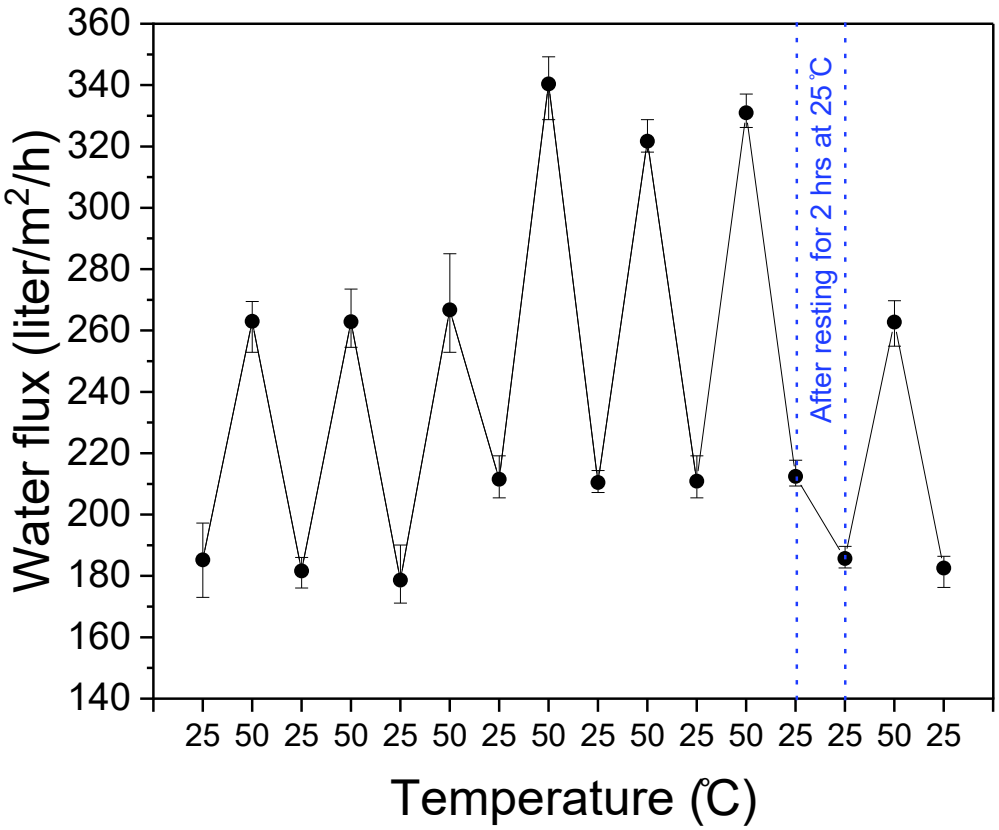

Fig. 5. Reversibility of the water flux of the polyLLC membrane under several heating-cooling cycles.

Reversibility of the response to an external stimulus is as important as stimuli-responsiveness since it determines the chemical and physical structural stability of the product after each response. In the next step, therefore, we evaluated the thermoreversibility behavior of polyLLC membrane. To

do so, the water flux of the membrane was measured at 25 and 50 °C repeatedly (under several heating-cooling cycles). The obtained results are shown in Fig. 5. The membrane exhibits excellent reversible behavior under 3 heating-cooling cycles. However, after the third cycle, the water flux becomes higher at both 25 and 50 °C, which remains unchanged with continuing the test for consecutive cycles. Irreversible change of molecular structure (e.g., washing out of F127 from the membrane) was the first speculation. However, the permeate was tested using TOC measurement method and no sign of F127 was observed. Also, the water flux returned to the original values after giving 2 h rest to the membrane at 25 °C. Based on this observation, it appears that the change in molecular structure after several heating-cooling cycles is reversible yet time-consuming.

3.2.3. Fouling resistance and cleaning efficiency

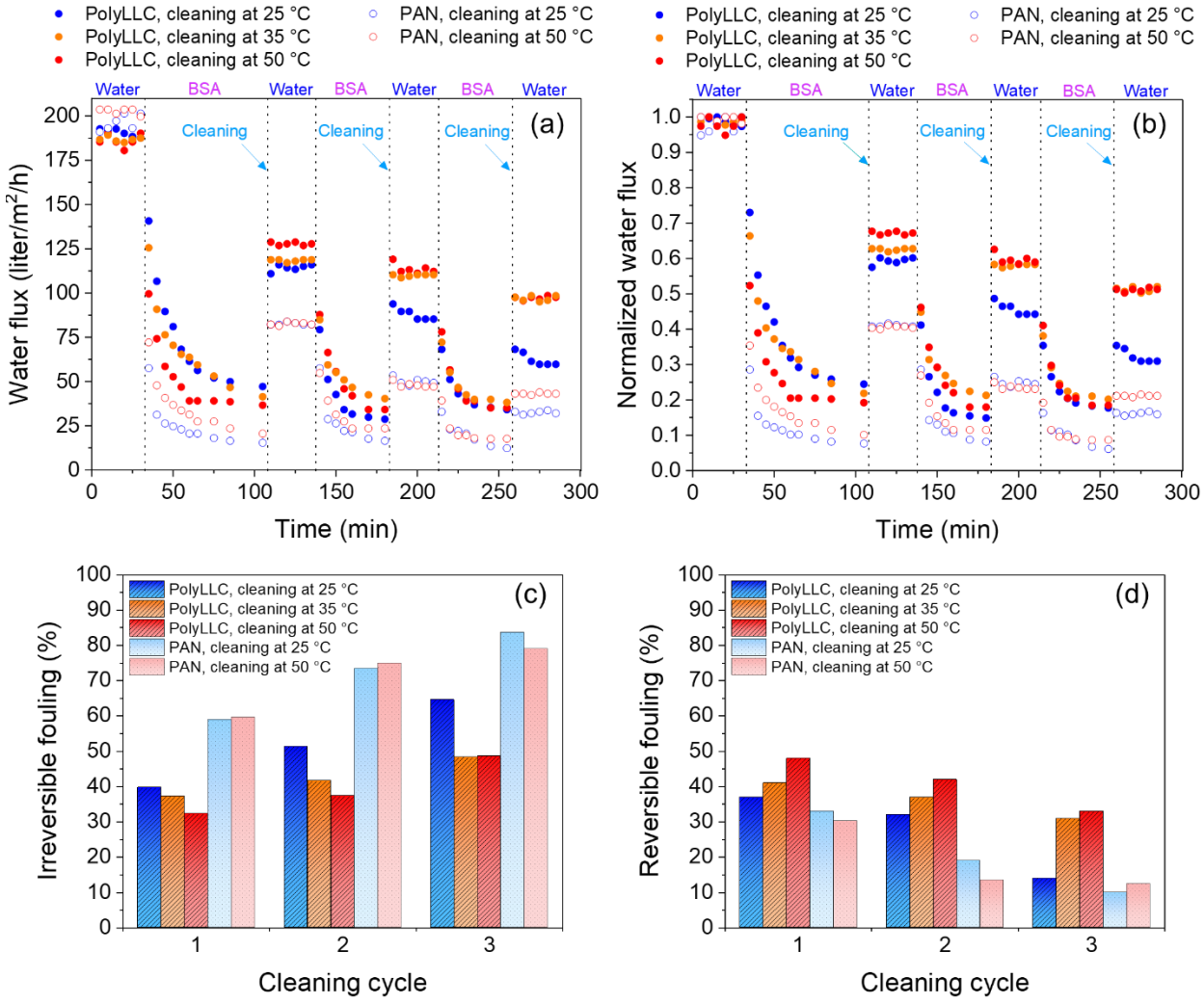

Fig. 6. Change of (a) water flux, (b) normalized water flux, (c) irreversible fouling, and (d) reversible fouling for polyLLC and PAN membranes throughout fouling-cleaning experiment using different cleaning temperatures. The presented temperatures are cleaning temperature and filtrations steps were carried out at 25℃.

As stated in the introduction section, enhancing the reversible fouling over irreversible fouling (also called cleaning efficiency) is one of the important advantages of thermoresponsive membranes. Hence, we performed fouling-cleaning experiments (see the experimental section) on the polyLLC membrane and PAN membrane (as control sample). To evaluate the cleaning efficiency for the polyLLC membrane, the cleaning steps were carried out at 25, 35 and 50 °C (all the filtrations steps were performed on BSA feed solution at 25 °C). In the case of the PAN membrane, we only did the cleaning at 25 and 50 °C. As shown in Fig. 6, the normalized water flux, which is obtained through dividing the measured flux at any time by the primary flux of the fresh membrane, has also been evaluated in addition to the water flux itself. Based on the obtained trends, polyLLC membrane exhibits a higher fouling resistance compared to PAN membrane as the irreversible fouling is much lower for the former.

According to the results presented in Fig. 6, the reversible fouling for polyLLC membrane increases with an increase in the cleaning temperature, whereas there is no improvement for the PAN membrane. Such improvement happens due to an increase in the porosity of polyLLC membrane with temperature, which can enhance the foulant removal. Another noticeable observation here is the significant difference in the reversible fouling of polyLLC membrane in the third cycle in the case of cleaning at 25 °C compared to 35 and 50 °C. This result implies that utilizing the thermoresponsiveness of polyLLC membrane can increase the cleaning efficiency and decrease the irreversible attachment of foulants, thus, increasing membrane lifetime.

3.2.4. Molecular weight cut-off

Manipulation of the membrane selectivity through an external stimulus is one of the important advantages of stimuli-responsive membranes. Having this feature depends on changing the membrane pore size in response to a stimulus. MWCO measurement is the common method used for determining the pore size of membranes. Therefore, we used this approach to evaluate the extent of pore size change of the polyLLC membrane in response to temperature. PEO solutions having different molecular weights were employed to measure the MWCO at 25, 35 and 50 °C. The acquired results are shown in Fig. 7. The MWCO of the membrane at room temperature is about 250 kDa from a sigmoidal fit on the rejection vs molecular weight data points in this figure. As presented in equation (7), Boltzmann sigmoidal equation has been used for the fitting MWCO behavior, where A_1, A_2, x_0, and m are initial value, final value, center, and slope, respectively:

$$y = A_2 + \frac{(A_1 - A_2)}{1 + e^{\frac{(x - x_0)}{m}}} \qquad (7)$$

By using equation (6), a pore size of ~30.8 nm can be calculated for the membrane at room temperature. The MWCO of the membrane increases to around 336 and 570 kDa with an increase in the temperature to 35 and 50 °C, respectively. These MWCOs are equal to pore sizes of ~36.6 and ~50 nm, respectively. The results prove the possibility of the pore size manipulation for polyLLC membrane, and thus, its selectivity. It is also noteworthy to point out that melting of crystalline structure at 50 °C has stronger effect on the porosity compared to LCST transition at

35 °C, which is in good agreement with the results of hydration capacity, permeability, and fouling-cleaning experiments.

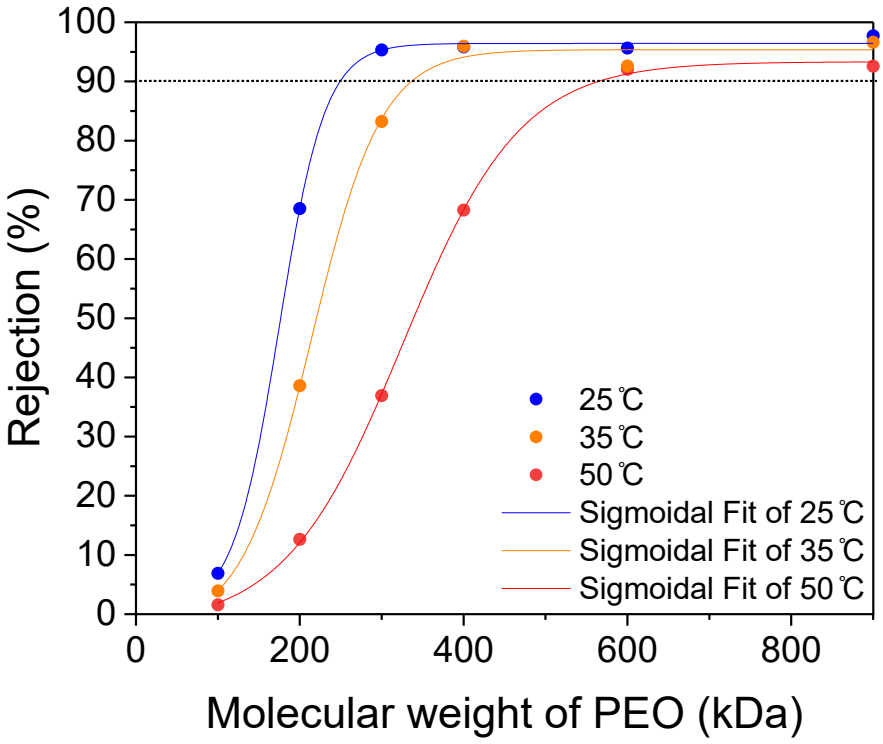

Fig. 7. Temperature-dependent MWCO of polyLLC membrane.

The effect of temperature on the size of PEO chains has not been considered in the pore size calculations mentioned in the above paragraph. Therefore, we measured the hydrodynamic radius of PEO chains with different molecular weights at 25, 35 and 50 °C using DLS analysis. Fig. 8 represents the obtained results (PEO chains size distribution can be found in Fig. S1). As can be seen, the size of PEO chains with different molecular weights slightly increases with an increase in the temperature, which shows that the solubility of the polymer enhances in water at high temperatures. The same results have been reported by Hammouda et al. for PEO chains with molecular weight of 36,500 g/mol using appropriate aqueous solution concentrations [39]. It should also be noted that PEO has an LCST in water in 100-180°C range (depending on molecular weight) [40], which is much higher than the temperature range used in our experiments. By interpolation of the obtained data, the pore size of the membrane can be calculated as 34.6 nm at room temperature which is in good agreement with the theoretical calculations. After correcting the pore size calculation with considering temperature effect, it appears that the pore size of polyLLC membrane increases to 45.7 and 59.6 nm at 35 and 50 °C, respectively.

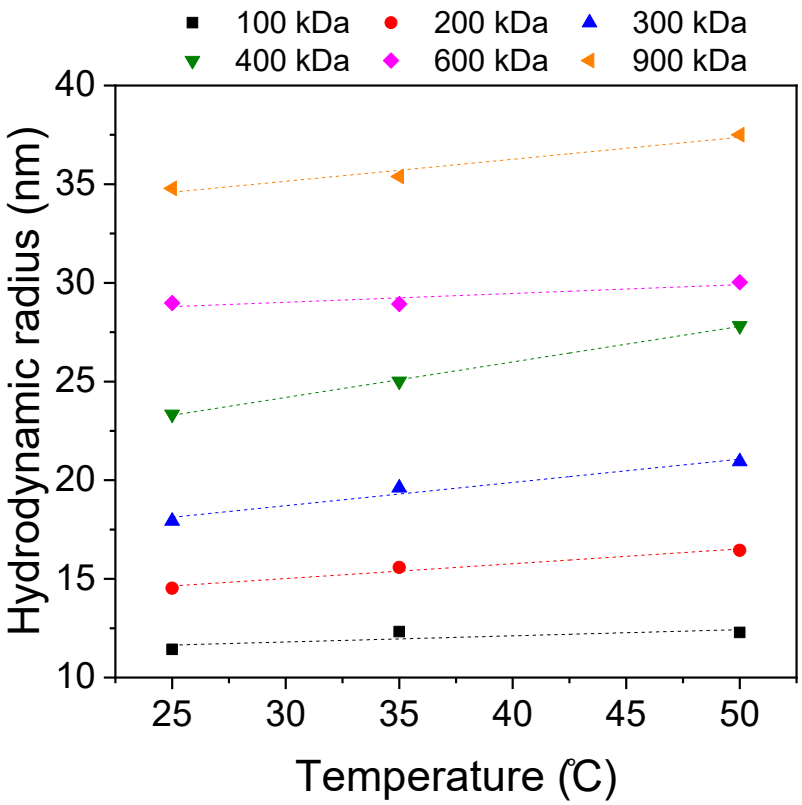

Fig. 8. Temperature-dependent chain size for PEO having different molecular weights.

3.3. Thermoresponsiveness mechanism of polyLLC membrane

According to the presented results, the studied polyLLC exhibits a two-step response with temperature changes. While elaboration of the response at 50 °C is relatively simple, explanation of the response at about 30 °C, which happens due to the LCST behavior of F127, is rather complicated. Before starting the discussion regarding this behavior in LLC nanostructure, it is required to have an understanding about the LCST behavior of F127, which is observed as sol-gel transition in aqueous media [41]. The sol-gel transition of F127 taking place in 25-37 °C is attributed to the aggregation of PPO block in water with an interconnected corona of PEO chains. This transition can be reversed by cooling down the formed gel [41]. Therefore, PPO block is responsible for the LCST behavior of F127 around 25-37 °C. In the reported works on LLCs and polyLLCs created by Pluronic surfactants, PPO block is suggested to be completely oriented towards the apolar domain [3,42–44]. It means that when the polymerization happens, PPO chains can be trapped inside the cross-linked polymer network near the interface. If the PPO block is responsible for the LCST behavior of the polyLLC studied in our work, having a dense cross-linked network can eliminate the first thermal transition observed in DSC diagrams by limiting the mobility of PPO chains. Additionally, as the LCST behavior takes place in the presence of water, the first thermal transition should not be detected via DSC when a dried polyLLC is examined. Based on these speculations, we carried out DSC on polyLLC samples containing 20, 50, 100, and 150 wt% EGDMA with respect to *n*BA content. Furthermore, we performed DSC on a dried

polyLLC containing 20 wt% EGDMA with respect to nBA content. The obtained results are shown in Fig. 9. As can be seen, the first thermal transition becomes weaker and then almost disappears as the cross-linker content is increased (area under the peak decreases from ~ 2.4 to ~ 0.5 J/g), while the second transition (PEO melting) remains intact (with an area under the peak of ~ 2.9 J/g). Moreover, there is no thermal transition around 30 °C for the dried polyLLC, whereas the transition at about 50 °C is stronger (area under the peak of ~ 42 J/g) for this sample compared to the wet one (area under the peak of ~ 2.9 J/g). This stronger peak can be attributed to the higher crystallinity of PEO blocks in the absence of water as the solvent. These results confirm our hypothesis that PPO block is responsible for the LCST behavior of F127 in polyLLC nanostructure.

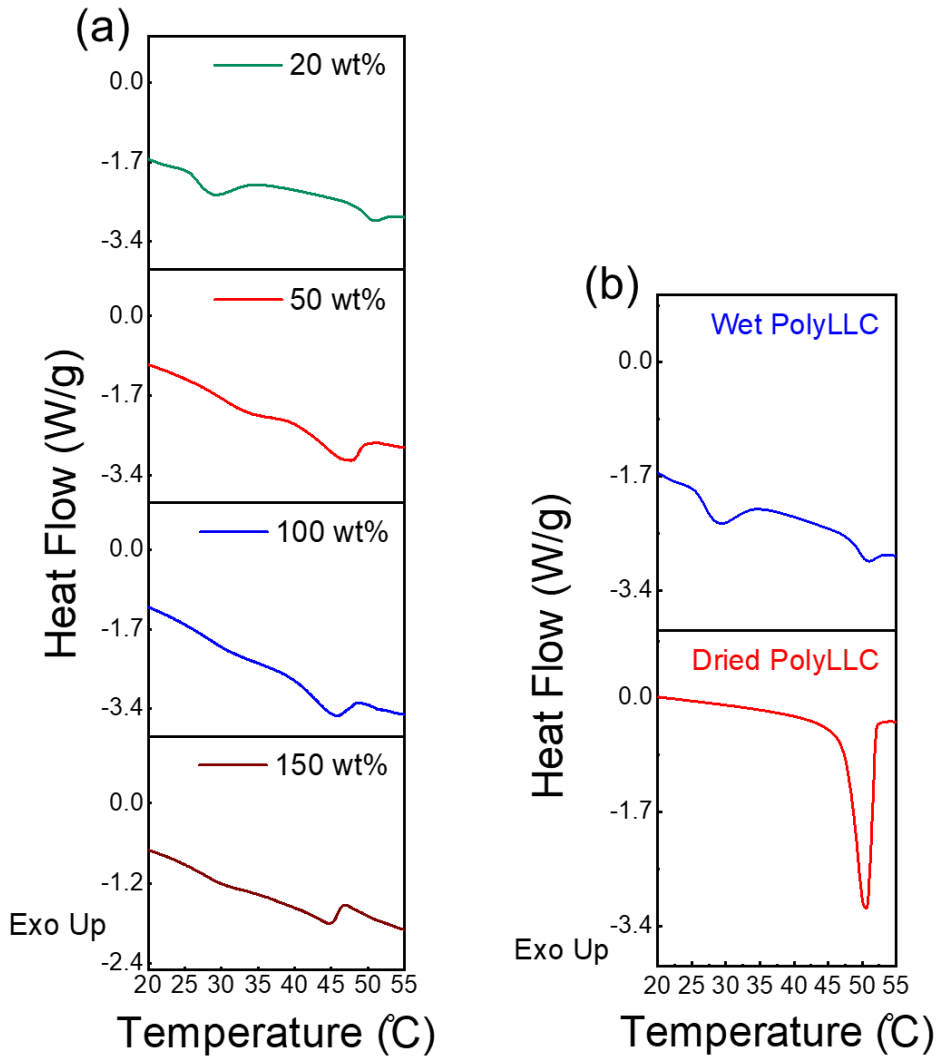

Fig. 9. Results of DSC measurement for (a) polyLLCs containing different cross-linker contents and (b) wet and dried polyLLC containing 20 wt% cross-linker with respect to *n*BA content.

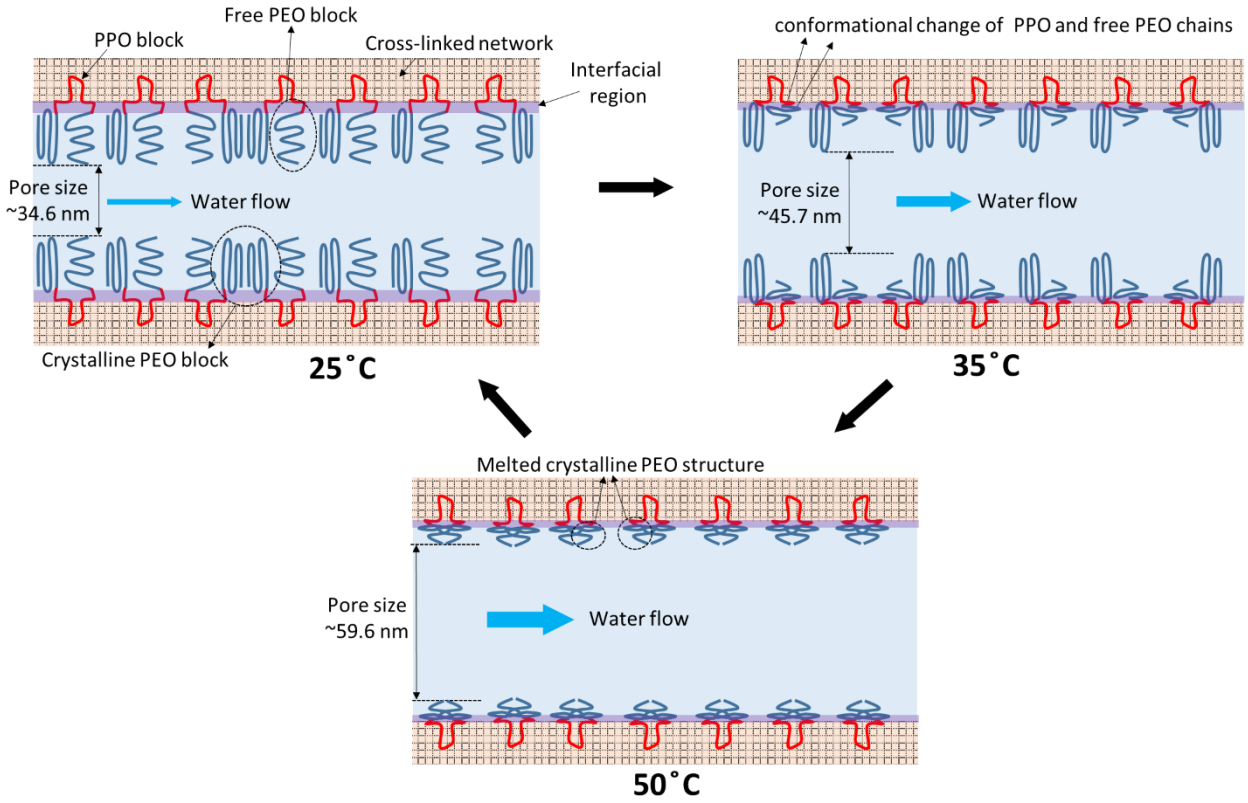

Fig. 10. Formation and thermoresponsiveness mechanism of polyLLC membrane.

According to the obtained results, the thermoresponsiveness mechanism of the polyLLC membrane can be elaborated as follows. A mesophase with lamellar structure is obtained via mixing F127, water, and polymerizable oil phase. The PPO blocks arrange themselves towards the oil phase and at the oil/water interface, while PEO blocks have a semi-crystalline structure in the water channels. The polymerization results in a cross-linked poly(nBA-co-EGDMA) network which holds PPO blocks at the interface of the polymer phase, thus, fixing F127 molecules in their position (negligible chance of their removal by water). With an increase in the temperature to 35 °C, PPO blocks start to rearrange themselves in a way to minimize their contact with water at the interface, resulting in dragging PEO blocks towards the water/polymer interface. Consequently, the membrane pore size increases from ~34.6 to ~45.7 nm. Further increasing the temperature to 50 °C melts down the crystalline structure of PEO block. The freed PEO chains now rearrange themselves near the polymer/water interface to form coating at the interface to cover the potential exposure of PPO blocks to water, similar to the discussed arrangement during sol-gel transition in aqueous media [41]. The pore size increase to ~59.6 nm is the result of such molecular rearrangements. All these transitions are reversible upon cooling the system to the room temperature. The explained mechanism is schematically shown in Fig. 10. We might also elaborate the increase in the water flux during thermoreversibility test by using this mechanism. It seems that the PEO blocks rearrange themselves much closer to the polymer/water interface when the membrane is under cyclic thermal load, probably due to the changes in steric restrictions (e.g.,

chain entanglements). This effect results in bigger pore size and thus higher flux. This behavior seems to be predominant for the PEO chains participating in the formation of crystals (which has slower kinetics) since the chains can retain their original semi-crystalline structure after enough resting time.

4. CONCLUSION

In this study, we reported a simple approach to fabricate two-step thermoresponsive UF membranes by polymerization of LLCs. Commercially available F127 with thermoresponsive property was used as an amphiphile to create lamellar structure in combination with water and hydrophobic monomers. After the polymerization, the formed cross-linked network fixed F127 molecules in their positions, preventing their removal by water. Hydration capacity, permeability, fouling resistance, cleaning efficiency, and MWCO of the fabricated membrane was evaluated. The experimental results revealed that the membrane exhibits two-step thermoresponsiveness at 35 °C due to the LCST of F127 and 50 °C thanks to the melting of PEO crystalline structure. Moreover, the MWCO measurements showed that the pore size of the membrane can be altered from 34.6 nm to 45.7 and 59.6 nm by increasing the temperature to 35 and 50 °C, respectively. The cleaning efficiency and thus lifetime of the membrane can be enhanced by cleaning the contaminated membrane at high temperatures due to the porosity change in response to the temperature. As future work, the fabrication of polyLLC functional materials can be extended to produce membranes with lower pore sizes in 1-15 nm range.

ACKNOWLEDGEMENTS

The authors would like to thank the support by the National Science Foundation (NSF) under grant no. 1840871. This work was performed, in part, at the Center for Integrated Nanotechnologies, an Office of Science User Facility operated for the U.S. Department of Energy (DOE) Office of Science. Los Alamos National Laboratory, an affirmative action equal opportunity employer, is managed by Triad National Security, LLC for the U.S. DOE's NNSA, under contract 89233218CNA000001.

CONFLICT OF INTEREST

The authors declare that they have no conflict of interest.

REFERENCES

[1] J.R. Werber, C.O. Osuji, M. Elimelech, Materials for next-generation desalination and water purification membranes, Nat. Rev. Mater. 1 (2016) 16018. https://doi.org/10.1038/natrevmats.2016.18.

[2] R.W. Baker, Membrane Technology and Applications, John Wiley & Sons, Ltd, Chichester, UK, 2012. https://doi.org/10.1002/9781118359686.

[3] S. Qavi, A.P. Lindsay, M.A. Firestone, R. Foudazi, Ultrafiltration membranes from polymerization of self-assembled Pluronic block copolymer mesophases, J. Memb. Sci. 580 (2019) 125–133. https://doi.org/10.1016/j.memsci.2019.02.060.

[4] A. Rektor, G. Vatai, Membrane filtration of Mozzarella whey, Desalination. 162 (2004) 279–286. https://doi.org/10.1016/S0011-9164(04)00052-9.
[5] A. Cassano, M. Marchio, E. Drioli, Clarification of blood orange juice by ultrafiltration: analyses of operating parameters, membrane fouling and juice quality, Desalination. 212 (2007) 15–27. https://doi.org/10.1016/j.desal.2006.08.013.
[6] Q. Li, Q. Bi, H.-H. Lin, L.-X. Bian, X.-L. Wang, A novel ultrafiltration (UF) membrane with controllable selectivity for protein separation, J. Memb. Sci. 427 (2013) 155–167. https://doi.org/10.1016/j.memsci.2012.09.010.
[7] X. Zhao, Y. Su, W. Chen, J. Peng, Z. Jiang, pH-responsive and fouling-release properties of PES ultrafiltration membranes modified by multi-functional block-like copolymers, J. Memb. Sci. 382 (2011) 222–230. https://doi.org/10.1016/j.memsci.2011.08.014.
[8] D. Wandera, S.R. Wickramasinghe, S.M. Husson, Stimuli-responsive membranes, J. Memb. Sci. 357 (2010) 6–35. https://doi.org/10.1016/j.memsci.2010.03.046.
[9] M.K. Sinha, M.K. Purkait, Preparation of a novel thermo responsive PSF membrane, with cross linked PVCL-co-PSF copolymer for protein separation and easy cleaning, RSC Adv. 5 (2015) 22609–22619. https://doi.org/10.1039/C4RA13863E.
[10] M.K. Sinha, M.K. Purkait, Preparation and characterization of novel pegylated hydrophilic pH responsive polysulfone ultrafiltration membrane, J. Memb. Sci. (2014). https://doi.org/10.1016/j.memsci.2014.03.067.
[11] J. Fu, X. Wang, Z. Ma, H. Wenming, J. Li, Z. Wang, L. Wang, Photocatalytic ultrafiltration membranes based on visible light responsive photocatalyst: a review, Desalin. WATER Treat. 168 (2019) 42–55. https://doi.org/10.5004/dwt.2019.24403.
[12] T. Xiang, T. Lu, W.-F. Zhao, C.-S. Zhao, Ionic strength- and thermo-responsive polyethersulfone composite membranes with enhanced antifouling properties, New J. Chem. 42 (2018) 5323–5333. https://doi.org/10.1039/C8NJ00039E.
[13] S. Darvishmanesh, X. Qian, S.R. Wickramasinghe, Responsive membranes for advanced separations, Curr. Opin. Chem. Eng. 8 (2015) 98–104. https://doi.org/10.1016/j.coche.2015.04.002.
[14] J.-Y. Choi, T. Yun, S.-Y. Kwak, Two-step thermoresponsive membrane with tunable separation properties and improved cleaning efficiency, J. Memb. Sci. 554 (2018) 117–124. https://doi.org/10.1016/j.memsci.2018.02.060.
[15] D. Roy, W.L.A. Brooks, B.S. Sumerlin, New directions in thermoresponsive polymers, Chem. Soc. Rev. 42 (2013) 7214. https://doi.org/10.1039/c3cs35499g.
[16] J.-Z. Yu, L.-P. Zhu, B.-K. Zhu, Y.-Y. Xu, Poly(N-isopropylacrylamide) grafted poly(vinylidene fluoride) copolymers for temperature-sensitive membranes, J. Memb. Sci. 366 (2011) 176–183. https://doi.org/10.1016/j.memsci.2010.09.055.
[17] X. Chen, S. Bi, C. Shi, Y. He, L. Zhao, L. Chen, Temperature-sensitive membranes prepared from blends of poly(vinylidene fluoride) and poly(N-isopropylacrylamides) microgels, Colloid Polym. Sci. 291 (2013) 2419–2428. https://doi.org/10.1007/s00396-013-2985-y.
[18] C. Kahrs, J. Schwellenbach, Membrane formation via non-solvent induced phase separation using sustainable solvents: A comparative study, Polymer. 186 (2020) 122071. https://doi.org/10.1016/j.polymer.2019.122071.
[19] X. Feng, Q. Imran, Y. Zhang, L. Sixdenier, X. Lu, G. Kaufman, U. Gabinet, K. Kawabata, M. Elimelech, C.O. Osuji, Precise nanofiltration in a fouling-resistant self-assembled membrane with water-continuous transport pathways, Sci. Adv. 5 (2019) eaav9308.

https://doi.org/10.1126/sciadv.aav9308.
[20] M. Zhou, T.J. Kidd, R.D. Noble, D.L. Gin, Supported lyotropic liquid-crystal polymer membranes: Promising materials for molecular-size-selective aqueous nanofiltration, Adv. Mater. 17 (2005) 1850–1853. https://doi.org/10.1002/adma.200500444.
[21] B.M. Carter, B.R. Wiesenauer, E.S. Hatakeyama, J.L. Barton, R.D. Noble, D.L. Gin, Glycerol-based bicontinuous cubic lyotropic liquid crystal monomer system for the fabrication of thin-film membranes with uniform nanopores, Chem. Mater. 24 (2012) 4005–4007. https://doi.org/10.1021/cm302027s.
[22] S.T. Hyde, Identification of Lyotropic Liquid Crystalline Mesophases, in: Handb. Appl. Surf. Colloid Chem., 2001: pp. 299–332.
[23] B.R. Wiesenauer, D.L. Gin, Nanoporous polymer materials based on self-organized, bicontinuous cubic lyotropic liquid crystal assemblies and their applications, Polym. J. 44 (2012) 461–468. https://doi.org/10.1038/pj.2012.15.
[24] E.S. Hatakeyama, B.R. Wiesenauer, C.J. Gabriel, R.D. Noble, D.L. Gin, Nanoporous, bicontinuous cubic lyotropic liquid crystal networks via polymerizable gemini ammonium surfactants, Chem. Mater. 22 (2010) 4525–4527. https://doi.org/10.1021/cm1013027.
[25] X. Feng, S. Nejati, M.G. Cowan, M.E. Tousley, B.R. Wiesenauer, R.D. Noble, M. Elimelech, D.L. Gin, C.O. Osuji, Thin polymer films with continuous vertically aligned 1 nm pores fabricated by soft confinement, ACS Nano. 10 (2016) 150–158. https://doi.org/10.1021/acsnano.5b06130.
[26] S.M. Dischinger, J. Rosenblum, R.D. Noble, D.L. Gin, K.G. Linden, Application of a lyotropic liquid crystal nanofiltration membrane for hydraulic fracturing flowback water: Selectivity and implications for treatment, J. Memb. Sci. 543 (2017) 319–327. https://doi.org/10.1016/j.memsci.2017.08.028.
[27] B.S. Forney, C. Baguenard, C. Allan Guymon, Improved stimuli-response and mechanical properties of nanostructured poly(N-isopropylacrylamide-co-dimethylsiloxane) hydrogels generated through photopolymerization in lyotropic liquid crystal templates, Soft Matter. 9 (2013) 7458–7467. https://doi.org/10.1039/c3sm50556a.
[28] J.R. McLaughlin, N.L. Abbott, C.A. Guymon, Responsive superabsorbent hydrogels via photopolymerization in lyotropic liquid crystal templates, Polymer. 142 (2018) 119–126. https://doi.org/10.1016/j.polymer.2018.03.016.
[29] S. Chatterjee, P.C. Hui, E. Wat, C. Kan, P.-C. Leung, W. Wang, Drug delivery system of dual-responsive PF127 hydrogel with polysaccharide-based nano-conjugate for textile-based transdermal therapy, Carbohydr. Polym. 236 (2020) 116074. https://doi.org/10.1016/j.carbpol.2020.116074.
[30] S. CHATTERJEE, P. Chi-leung HUI, Review of Stimuli-Responsive Polymers in Drug Delivery and Textile Application, Molecules. 24 (2019) 2547. https://doi.org/10.3390/molecules24142547.
[31] S. Chatterjee, P.C. Hui, C. Kan, W. Wang, Dual-responsive (pH/temperature) Pluronic F-127 hydrogel drug delivery system for textile-based transdermal therapy, Sci. Rep. 9 (2019) 11658. https://doi.org/10.1038/s41598-019-48254-6.
[32] P. Holmqvist, P. Alexandridis, B. Lindman, Modification of the Microstructure in Poloxamer Block Copolymer−Water−"Oil" Systems by Varying the "Oil" Type, Macromolecules. 30 (1997) 6788–6797. https://doi.org/10.1021/ma970625q.
[33] S. Thakral, K. Kim, Small-angle scattering for characterization of pharmaceutical materials, TrAC Trends Anal. Chem. 134 (2021) 116144.

https://doi.org/10.1016/j.trac.2020.116144.
[34] R. C. Weast, CRC Handbook of Chemistry and Physics, 64th ed., CRC Press, Boca Raton, FL, 1983.
[35] C.J. Davey, Z.-X. Low, R.H. Wirawan, D.A. Patterson, Molecular weight cut-off determination of organic solvent nanofiltration membranes using poly(propylene glycol), J. Memb. Sci. 526 (2017) 221–228. https://doi.org/10.1016/j.memsci.2016.12.038.
[36] D.L. Ho, B. Hammouda, S.R. Kline, Clustering of poly(ethylene oxide) in water revisited, J. Polym. Sci. Part B Polym. Phys. 41 (2003) 135–138. https://doi.org/10.1002/polb.10340.
[37] Y. Huang, S. Gui, Factors affecting the structure of lyotropic liquid crystals and the correlation between structure and drug diffusion, RSC Adv. 8 (2018) 6978–6987. https://doi.org/10.1039/c7ra12008g.
[38] S. Singh, K.. Khulbe, T. Matsuura, P. Ramamurthy, Membrane characterization by solute transport and atomic force microscopy, J. Memb. Sci. 142 (1998) 111–127. https://doi.org/10.1016/S0376-7388(97)00329-3.
[39] B. Hammouda, D.L. Ho, Insight into chain dimensions in PEO/water solutions, J. Polym. Sci. Part B Polym. Phys. 45 (2007) 2196–2200. https://doi.org/10.1002/polb.21221.
[40] V.Y. Grinberg, T. V. Burova, N. V. Grinberg, A.S. Dubovik, V.S. Papkov, A.R. Khokhlov, Energetics of LCST transition of poly(ethylene oxide) in aqueous solutions, Polymer. 73 (2015) 86–90. https://doi.org/10.1016/j.polymer.2015.07.032.
[41] A.M. Deliormanlı, M. Türk, Flow Behavior and Drug Release Study of Injectable Pluronic F-127 Hydrogels containing Bioactive Glass and Carbon-Based Nanopowders, J. Inorg. Organomet. Polym. Mater. 30 (2020) 1184–1196. https://doi.org/10.1007/s10904-019-01346-2.
[42] P. Alexandridis, U. Olsson, B. Lindman, Self-Assembly of Amphiphilic Block Copolymers: The (EO)13(PO)30(EO)13-Water-p-Xylene System, Macromolecules. 28 (1995) 7700–7710. https://doi.org/10.1021/ma00127a016.
[43] S. Qavi, A. Bandegi, M. Firestone, R. Foudazi, Polymerization in soft nanoconfinement of lamellar and reverse hexagonal mesophases, Soft Matter. 15 (2019) 8238–8250. https://doi.org/10.1039/c9sm01565e.
[44] A. Bandegi, J.L. Bañuelos, R. Foudazi, Formation of ion gels by polymerization of block copolymer/ionic liquid/oil mesophases, Soft Matter. 16 (2020) 6102–6114. https://doi.org/10.1039/D0SM00850H.